Eduard Marenić
Jurica Sorić
Zdenko Tonković

NANO-SUBMODELLING TECHNIQUE BASED ON OVERLAPPING DOMAIN DECOMPOSITION METHOD

Summary

A multiscale method that couples an atomistic with a continuum model is presented. Nano-submodelling (nSM) is an approach that enables the insertion of a nano-refined submodel (atomistic) in a global model (continuum). The applied concurrent atomistic-to-continuum coupling of the two models is based on the overlapping domain decomposition scheme called the bridging domain method or on a similar method, the Arlequin method. Different models overlap and the displacement compatibility is enforced via Lagrange multipliers. In this study, an analysis of the spurious effects that may arise in and near the coupling domain is performed. Some coupling options such as energy weighting, coupling zone geometry, and the Lagrange multiplier field interpolation are tested.

Key words: molecular mechanics, multiscale, ghost forces, atomistic-to-continuum coupling, bridging domain method.

1. Introduction

Submodelling is a common engineering technique usually implemented in standard finite element (FE) method codes. It is used for detailed study of various geometrical discontinuities like grooves, welds, notches, and cracks. For example, in [1], calculations of the stress intensity factor and the J-integral of cracked structural components are performed by using the submodelling technique. Therein, the results from the global model are interpolated on the boundary of the submodel. The global model has a relatively coarse mesh without a crack, and the submodel consists of a fine mesh with a crack.

Mesh refinement in the local-global strategy is selective and is carried out only on local subdomains without gradual transition. Only locally refined mesh considerably reduces the computational time. The s-method [2] is an example of the local-global type multimodel framework that superimposes additional refined meshes to the existing global one. Another example is the Arlequin method [3–5] where the FE models are not added but they partially overlap and are glued to each other. The fact that models are locally crossed with each other allows the coexistence of substantially different mechanical and mathematical models [3], and hence this approach can be used for multiscale modelling. Regarding coupling conditions between two scales, multiscale modelling approaches are divided into hierarchical (weak) and concurrent (strong) [6]. In the first approaches, the computations are performed on each scale separately and the scale coupling is often done by transferring the problem parameters leading to the classical problem of homogenization (*e.g.* see early work [7]). In the concurrent coupling of scales, the behavior of each scale strongly depends on the other, and the appropriate model is solved on each scale simultaneously [8]. Here, we focus on the concurrent, atomistic-to-continuum multiscale modelling, strongly coupling atomistic and continuum scales. A good example of the application of this kind of multiscale modelling is material failure which is often initiated by nano-defects that exist on the atomistic scale and cannot be described on the continuum scale (fracture is intrinsically an interatomic bond breaking phenomenon). Fully

atomistic (or molecular) simulations, with current computer resources, still remain out of reach for engineering systems of practical interest. Hence, extensive work has been done in the development of atomistic-to-continuum multiscale modelling approaches starting with [9] and [10]. An overview is given in [11–13] and a comparison of the methods performance in [14].

In this paper Belytschko's bridging domain (BD) [15–17] (or adopted the Arlequin method [18, 19]) is used for the atomistic-to-continuum coupling. These two methods are basically the same and are based on the overlapping domain decomposition (ODD) approach. Two different and partially overlapped domains are coupled, which enables the application of the nano-submodelling (nSM) technique *i.e.* the insertion of the nano-submodel in the global FE model. The coupling based on the ODD method differs in the following options: 1. definition of coupling zone, 2. choice of linking parameters (*e.g.* continuity of displacement, displacement derivatives and forces), 3. way to impose linking (Lagrange method, augmented Lagrange method [15]) and 4. energy distribution in the overlapping zone.

The paper is organized as follows. The governing equations and the coupling are described in section 2. In section 3, the performance of some of the mentioned coupling options is numerically tested. The numerical investigation is performed on a 1D academic example with the local and non-local interaction in the atomistic domain. Different options for energy weighting in the domain overlap and the Lagrange multiplier (LM) interpolation are studied together with its influence on coupling accuracy. Finally, some concluding remarks including further research plans are given in section 4.

2. Governing equations and coupling in nSM technique

The scheme of the coupled model domain Ω consisting of three subdomains is shown in Fig. 1. The atomistic domain Ω^a is treated with molecular mechanics (MM), whereas the continuum domain Ω^c is discretized by FEs. The role of the continuum model is to replace the molecular model with a coarser, and thus cheaper, model in $\Omega^c \subset \Omega$ away from the region of interest, *e.g.* crack or dislocation. Linear elasticity is selected for the continuum model assuming small deformations. The atomistic and continuum domains overlap on $\Omega^b = \Omega^a \cap \Omega^c$ which is called the bridging domain. This overlapping domain is also called the handshake or coupling domain. Traction $\bar{\mathbf{t}}$ and displacement boundary conditions $\bar{\mathbf{u}}$ are given on the part of the surface $\partial_t\Omega$ and

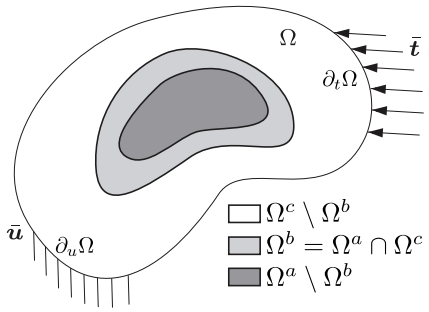

Fig. 1 Scheme of the coupled model and the nSM technique.

the complementary part of the surface $\partial_u\Omega$, respectively. Since $\partial_t\Omega$, $\partial_u\Omega \subset \Omega^c$, the treatment of the boundary conditions is standard as in the continuum FEM.

Total potential energy of the system may be written as

$$E_{tot,w} = E^c_w(\mathbf{u}) + E^a_w(\mathbf{d}) - E^{ext}(\mathbf{u}, \mathbf{d}), \tag{1}$$

where $\mathbf{u}$ i $\mathbf{d}$ are displacement vectors in the continuum and atomistic domain, respectively. Furthermore, E^{ext} is the work of external forces, while E_w^c and E_w^a are weighted continuum and atomistic energies, defined as

$$E_w^c(\mathbf{u}) = \int_{\Omega^c} w^c(\mathbf{X}) W(\mathbf{F})\, d\Omega^c, \qquad E_w^a(\mathbf{d}) = \frac{1}{2} \sum_{i,j \in \Omega^a} w^a V_{ij}. \tag{2}$$

In the above equations, $W(\mathbf{F})$ stands for the continuum strain energy density as a function of the deformation gradient $\mathbf{F}$, V_{ij} describes the atomistic interaction (bonding energies) where subscripts i and j indicate atom pairs in the two-body potential. In the bridging domain the atomistic and continuum models overlap, and the weighting functions w^c and w^a in (2) partition the energy. The weighting function serves to blend the behavior from the continuum model (w^c) and the atomistic model (w^a) and to avoid the double counting of the energy in the bridging domain. Furthermore, the use of an overlapping subdomain obviates the need for the FE nodes of the continuum model to correspond to the atomic positions. Thus, the finite element mesh does not need to be refined to the lattice dimensions around the atomistic subdomain, which is consistent with the nSM concept. The weighting functions w^c and w^a define a *partition of unity* of the energy in the bridging domain as follows:

$$\begin{aligned} w^c(\mathbf{X}) &= 1 \quad \text{for } \mathbf{X} \in \Omega^c \setminus \Omega^b, \\ w^a(\mathbf{X}) &= 1 \quad \text{for } \mathbf{X} \in \Omega^a \setminus \Omega^b, \\ w^c(\mathbf{X}) + w^a(\mathbf{X}) &= 1 \quad \text{for } \mathbf{X} \in \Omega^b. \end{aligned} \tag{3}$$

The coupling of the atomistic and continuum models is achieved by forcing displacement compatibility in the bridging domain as $\mathbf{u}(\mathbf{X} = \mathbf{X}_i) = \mathbf{d}_i$, $\forall i \in \Omega^b$. The Lagrange multiplier method is used to convert the problem of constrained minimization into finding the minimum of the larger, unconstrained problem. Hence, LMs, $\boldsymbol{\lambda}$, are used to enforce the compatibility between the discrete atomistic displacement and the continuum displacement field, which gives the following Lagrangian

$$W_L = E_{tot,w} + G = E_{tot,w} + \sum_{i \in \Omega^b} \int_{\Omega^b} \boldsymbol{\lambda}(\mathbf{X}) \cdot [\mathbf{u}(\mathbf{X}) - \mathbf{d}_i]\, \delta(\mathbf{X} - \mathbf{X}_i) \mathrm{d}\Omega, \tag{4}$$

where G is the constraint in terms of the energy, and $\delta(\mathbf{X} - \mathbf{X}_i)$ is the Dirac delta function.

Regarding the numerical implementation, the displacement field in Ω^c and LM fields in Ω^b are approximated by the shape functions $N_i(\mathbf{X})$ and $N_k^\lambda(\mathbf{X})$ as

$$\mathbf{u}(\mathbf{X}) = \sum_{i \in \mathcal{S}} N_i(\mathbf{X}) \mathbf{u}_i, \quad \boldsymbol{\lambda}(\mathbf{X}) = \sum_{k \in \mathcal{S}^\lambda} N_k^\lambda(\mathbf{X}) \hat{\lambda}_k, \tag{5}$$

with $\mathbf{u}_i$ and $\hat{\lambda}_k$ as nodal values. The set of all FE nodes is represented with $\mathcal{S}$, and $\mathcal{S}^\lambda$ is the set of all λ-nodes. The equilibrium configuration corresponds to the stationary point of the Lagrangian. The discrete equilibrium equations are obtained from the stationarity of the Lagrangian 4 with respect to $\mathbf{u}_i$, $\mathbf{d}_i$ and $\hat{\lambda}_i$:

$$\frac{\partial W_L}{\partial \mathbf{u}_i} = \frac{\partial E_w^c}{\partial \mathbf{u}_i} - \frac{\partial E_w^{ext}}{\partial \mathbf{u}_i} + \frac{\partial G}{\partial \mathbf{u}_i} = 0 \qquad \forall i \in \mathcal{S}, \tag{6}$$

$$\frac{\partial W_L}{\partial \mathbf{d}_i} = \frac{\partial E_w^a}{\partial \mathbf{d}_i} - \frac{\partial E_w^{ext}}{\partial \mathbf{d}_i} + \frac{\partial G}{\partial \mathbf{d}_i} = 0 \qquad \forall i \in \mathcal{M}, \tag{7}$$

$$\frac{\partial W_L}{\partial \hat{\lambda}_i} = \frac{\partial G}{\partial \hat{\lambda}_i} = 0 \qquad \forall i \in \mathcal{S}^\lambda. \tag{8}$$

In (7) $\mathcal{M}$ denotes the set of all atoms. The derivatives of the above equations give the forces, where uppercase $\mathbf{F}$ is used for continuum and lowercase $\mathbf{f}$ stands for the atomistic forces (indices int and ext refer to internal and external, respectively) as follows

$$\frac{\partial E_w^c}{\partial \mathbf{u}_i} = \mathbf{F}_i^{int}, \qquad \frac{\partial E_w^a}{\partial \mathbf{d}_i} = \mathbf{f}_i^{int}, \tag{9}$$

$$\frac{\partial E_w^{ext}}{\partial \mathbf{u}_i} = \mathbf{F}_i^{ext}, \qquad \frac{\partial E_w^{ext}}{\partial \mathbf{d}_i} = \mathbf{f}_i^{ext}. \tag{10}$$

3. Numerical investigation of one-dimensional coupling

3.1. Model description, nomenclature and symmetry boundary condition

According to the general scheme from Fig. 1, a chain-like one-dimensional (1D) model is used as a numerical example, see Fig. 2 a). The lengths l_a, l_c and l_b are simplified 1D counterparts of Ω^a, Ω^c and Ω^b respectively. The given parameters for the numerical examples considered in the following sections are: $l_0 = 1$, $l_b = 16l_0$, $l_a = 80l_0$, $l_c = 64l_0$. The size of the FE is denoted as l_e, and all the lengths are taken as the integer multiple of the lattice size l_0. Parameter R_c defines the cut-off radius which governs the atomistic potential interaction. In order to represent the real material adequately, the potential that governs the atomistic interaction should be extended beyond the nearest neighbour atoms. The potentials are thus non-local, in theory extending over the whole space but in practical implementations extending over a range R_c on the order of the first few neighbour distances. In this paper, the harmonic potential [20–24] is considered only, with the nearest and the second nearest neighbor interaction represented by the springs k_1 and k_2, respectively. Due to the practical implementation, in classical atomistic potentials, the total atomistic energy is partitioned into energies on a per-atom basis, even though the quantum energy cannot be treated in this manner [11]. The i-th atom scaled energy in the 1D case is

$$E_{w,i}^a = \frac{1}{2}\left[w_{i,i-1}^a \frac{k_1}{2}(d_i - d_{i-1})^2 + w_{i,i+1}^a \frac{k_1}{2}(d_{i+1} - d_i)^2 + w_{i,i-2}^a \frac{k_2}{2}(d_i - d_{i-2})^2 + w_{i,i+2}^a \frac{k_2}{2}(d_{i+2} - d_i)^2 \right]. \tag{11}$$

In the above equation the half in front of the bracket is to avoid double counting when summing up the terms to obtain the total atomistic energy $E^a = \sum_i E_i^a, \forall i \in \Omega^a$. The leftmost atom is

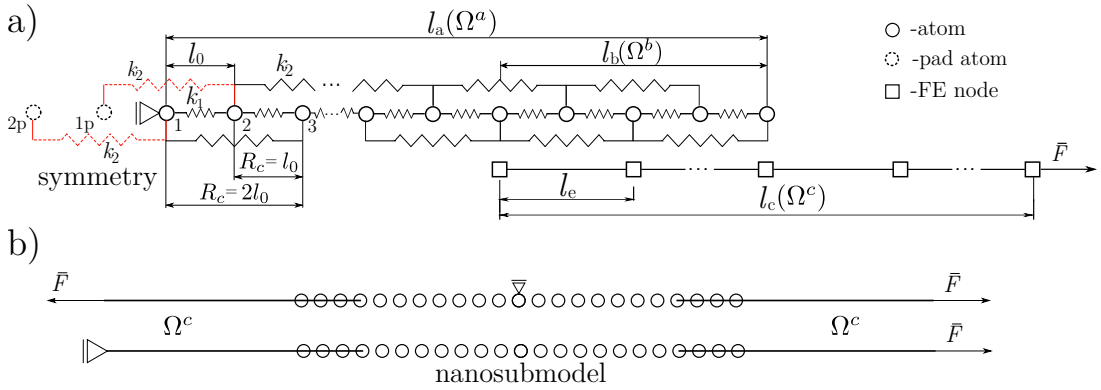

Fig. 2 1D coupling model scheme with the symmetry BC on the left end of the atomistic domain a). The utilization of the symmetry BC yields the configuration equivalent to the nSM inserted into the continuum chain b).

fixed and the rightmost node is loaded with $\bar{F} = 1$. The symmetry boundary condition (BC) is set (see Fig. 2 a) on the left), which corresponds to the nSM inserted in the continuum chain as presented in Fig. 2 b). The symmetry is modelled by including the energy of the pad atoms, *i.e.* the energy of the dashed springs k_2 connecting the pad atoms 1p and 2p with the atoms 1 and 2. The displacements of the pad atoms 1p and 2p are mirrored displacements of the atoms 2 and 3, respectively, so the energy is doubled. This remedy corrects the boundary effect on the left edge of the atomistic domain with the non-local interaction in the atomistic domain, see Fig. 3. When the pad atoms are not included in the total atomistic energy, the atoms 1 and 2 do not have non-local neighbours to the left. This causes errors *i.e.* oscillations in the strain field (Fig. 3). However, it should be noted that this effect does not occur when the interaction in the atomistic domain is local.

Apart from preventing boundary effects, the purpose of the symmetry is to obtain the configuration equivalent to the nSM inserted into the continuum chain (Fig. 2 b). The symmetry BC is used to avoid modelling of two bridging zones, one on the left and one on the right end of the nano-submodel. This remedy gives simple model which is needed to properly analyze the coupling and the errors that occur in and near the bridging zone.

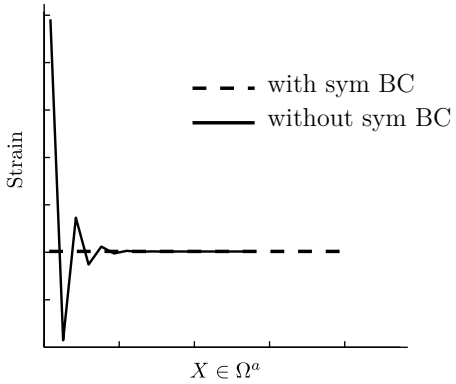

Fig. 3 Strain distribution plot for non-local interaction. The symmetry BC corrects the boundary effect and gives the constant strain field.

3.2. On the Lagrange multipliers and energy weighting

Two limiting cases regarding the LM field (see eq. (5)) are taken into consideration: the strict (also called non-interpolated) coupling where the LMs coincide with atoms *i.e.* $N_k^\lambda(\mathbf{X}_i) = \delta_{ki}$, and the interpolated coupling where the λ-nodes are coincident with FE nodes and the LM shape functions N_k^λ correspond to the FE shape functions N_k. The distribution of the λ-nodes for the two cases is shown in Fig. 4.

The FE size is taken as an integer multiple of the lattice size l_0 as mentioned, and the uniform meshes are considered only. The idea of the nSM technique is to avoid mesh refinement and to have a relatively coarse mesh, that is one or at most two elements in the bridging zone. However for the sake of analysis of atomistic-to-continuum coupling accuracy, the size of the FE is in the range from the lattice dimension to the size of the bridging zone, $l_e = l_0 \ldots l_b$. This is encompassed by the parameter $ES = 0 \ldots 1$ which defines the relative size of the FE element with respect to the size of the bridging zone:

$$ES(l_e) = \frac{l_e - l_0}{l_b - l_0} = \begin{cases} 1 & \text{for} \quad l_e = l_b, \\ 0 & \text{for} \quad l_e = l_0. \end{cases} \tag{12}$$

The FE size which is less than the lattice dimension is inconvenient in the sense of the nSM technique and is not studied here.

The energy weighting functions are varied and are taken to be constant (value 0.5), linear (ramp) and cubic functions of x in Ω^b as depicted in Fig. 5. The distribution of the three atomistic weighting functions w^a is shown, and due to simplicity, only the linear continuum weighting function (dashed line in Fig. 5) is shown.

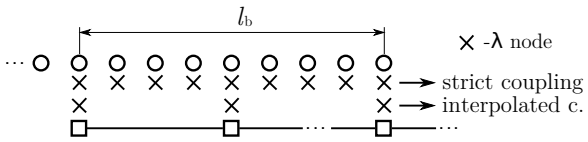

Fig. 4 Scheme of the distribution of the LM nodes for strict and interpolated coupling.

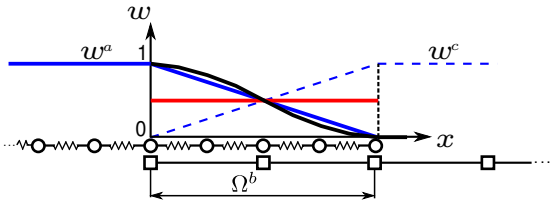

Fig. 5 Energy weighting function distribution in the bridging zone.

3.3. Strict coupling

The strict coupling is an expensive option which generates a new unknown for every atomistic DOF in Ω^b, as shown in Fig. 4. In 1D examples the number of additional unknowns, namely LMs, $n_\lambda = n_{ab}$, where n_{ab} is the number of atoms in the bridging zone. However, it will be shown that the strict coupling is more accurate. In fact, it exactly reproduces results from full molecular simulation for examples studied herein concerning the local and non-local atomistic interaction.

As the first example, the simplest molecular system with the local atomistic interaction is considered. The local or 1^{st} neighbour interaction implies $R_c = l_0$ or $k_1 = 1$ and $k_2 = 0$ in (11). The displacement and strain distribution are depicted in Fig. 6. For this simple molecular system the coupling is consistent and the model passes the patch test, *i.e.* it is able to reproduce a constant strain field exactly. For the local interaction in Ω^a and strict coupling, the constant strain field is obtained for any FE size ES or weighting function. Although it is not shown in this study, the exact strain field is obtained for any bridging size l_b, too. However, the LM field depends on the weighting function which is depicted in Fig. 7. For this very simple molecular model by hand calculation of the LM is carried out in [2, 25]. It is easy to show that $\lambda_i \propto (w^a_{i,i-1} - w^a_{i,i+1})$. Since $l_0 = 1$ the LM distribution for the local interaction corresponds to the first derivative of the weighting functions, *e.g.* the LM for the constant weighting function is zero in Ω^b except on the boundary, see Fig. 7.

In the next example, the non-local interaction is modelled in Ω^a by setting $R_c = 2l_0$, *i.e.* $k_1 = k_2 = 1$. For the non-local interaction case the accuracy depends on the strategy of calculating the atomistic weighting function $w^a_{i,j}$ from eq. (11). In Zhang et al. [26], the bonds are weighted by using the linear interpolation between an atom pair, which will be labeled here as *strategy A*

$$w^a_{i,j} = \frac{w^a(X_i) + w^a(X_j)}{2}. \tag{13}$$

In the original BD method [16], and *e.g.* in [27], the weighting function is calculated exactly at the half distance, denoted as *strategy B*

$$w^a_{i,j} = w^a\left(\frac{X_i + X_j}{2}\right). \tag{14}$$

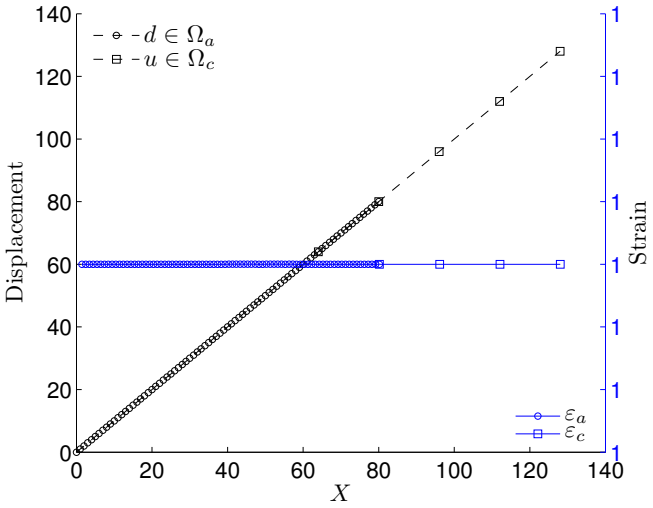

Fig. 6 Displacement and strain plots versus position for $R_c = l_0$, $k_1 = 1$ and $ES = 1$.

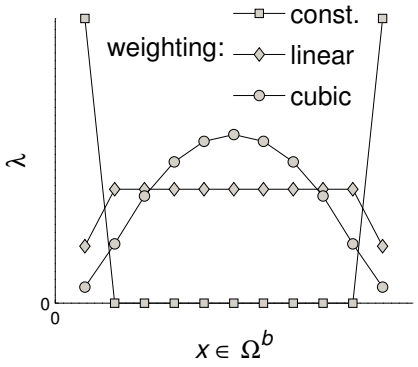

Fig. 7 Dependence of the LM in Ω^b for strict, local coupling.

The weighting using strategy A (13) yields some errors, as it can be seen in Fig. 8. Oscillations in the strain and small deviation in the deformed shape (not shown here) is due to ghost forces (GFs). GFs is a common name for the unphysical, spurious effect that occurs because of the locally affected symmetry of the global stiffness matrix [11, 28]. Fig. 8 shows that strain error highly depends on weighting strategy. For the constant weighting function the strain error is unacceptable, more than 50%, whereas it drops below 2.5% and 0.5% if the linear and cubic functions are used. On the other hand, the strict coupling and the weighting strategy B reproduce a constant strain field and yield no error for any weighting function or FE size (ES).

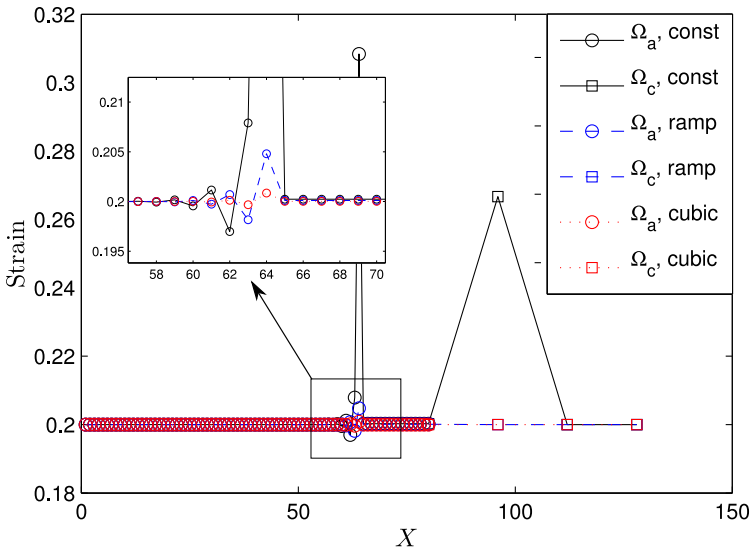

Fig. 8 Strain distribution for $R_c = 2l_0$, $ES = 1$, strict coupling, weighting strategy type A, with the weighting function varied.

3.4. Interpolated coupling

The interpolated coupling, where λ-nodes are coincident with FE nodes is computationally cheaper than the strict coupling, but consequently less accurate. In 1D examples $n_\lambda = n_{cb}$, where n_{cb} is the number of FE nodes in bridging zone, (see Fig. 4). The main idea of the nSM technique is to replace the molecular model with a much coarser continuum model, *i.e.* to achieve that $n_{cb} \ll n_{ab}$. This is not so obvious in the 1D case but it becomes so in the 2D and especially in the 3D case.
The exact distribution of the LM field for the strict, local atomistic interaction, shown in Fig. 7, does not change with the number of elements in the bridging zone. It is clear that for the interpolated coupling case, where $N_\lambda = N$, the LM distribution changes and considerably varies with the FE size (ES), as shown in Fig. 9. The limiting case $ES = 0$, clearly, gives the exact LM distribution, see Figs. 7 and 9, and is equivalent to the strict coupling. Inability

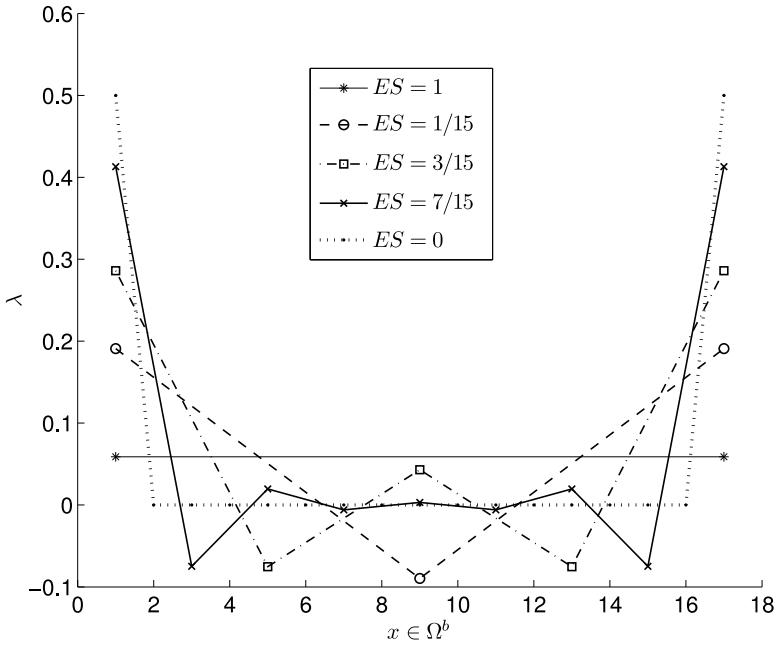

Fig. 9 Values of LMs for local interaction, interpolated coupling and constant weighting with different FE sizes (ES).

to reproduce an exact LM field for the case of the interpolated coupling (even for the local interaction) causes discrepancy from the constant strain field, see Fig. 10.

As for the strict coupling, the model with the non-local, harmonic interaction in the atomistic domain is studied for the interpolated case, too. The weighting strategy B is used here. This model causes even more significant oscillations in the strain field. This is expected because the interpolated coupling for the local interaction yielded errors, and adding non-locality only degrades the accuracy. However, no significant deviation from the linear displacement field can be noted, Fig. 11. The strain error caused by the coupling and due to GFs is a localized effect which is influencing the strain neither in the atomistic nor in the continuum domain.

4. Conclusion

Nano-submodelling is a multiscale method that combines the atomistic with the continuum model and seizes the benefits of the submodelling as a common engineering technique for inserting the refined submodel in the global model. In the nSM, the atomistic submodel is inserted

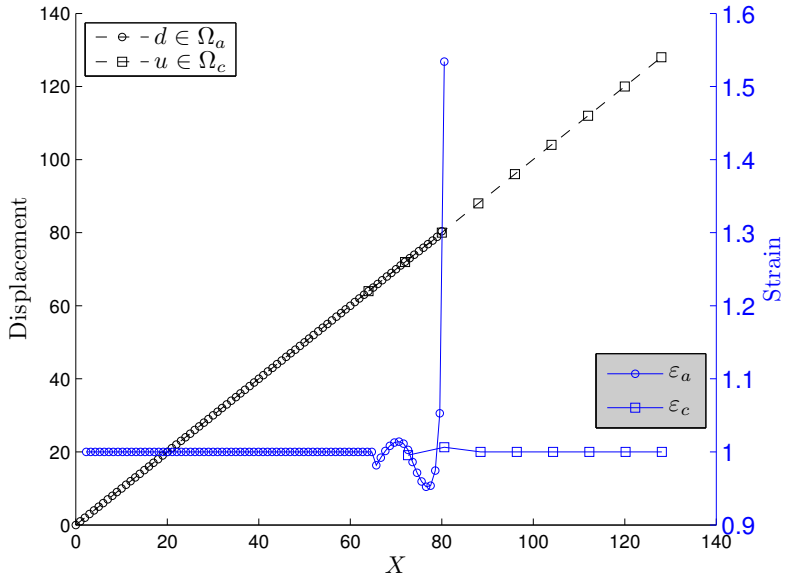

Fig. 10 Displacement and strain plots versus position for the local, interpolated coupling, with 2 elements per Ω^b ($ES = 1/15$).

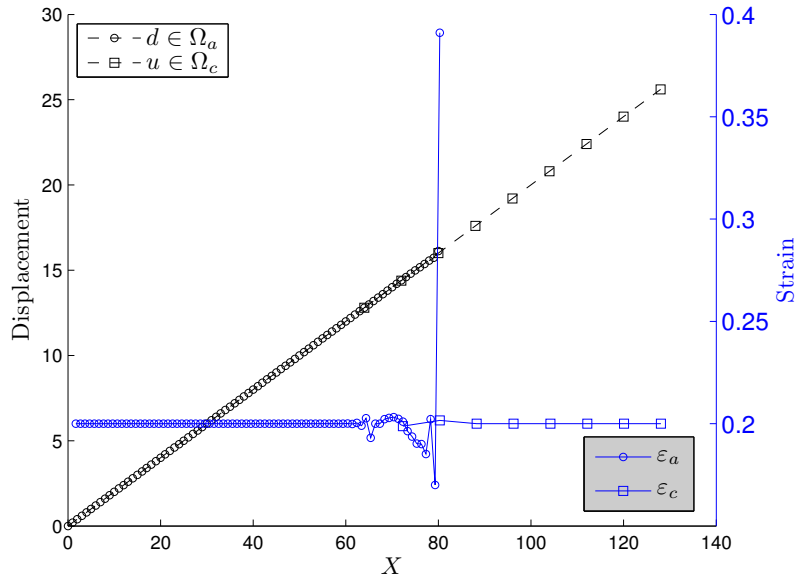

Fig. 11 Displacement and strain plots versus position for the non-local, interpolated coupling, with 2 elements per Ω^b ($ES = 1/15$).

in the global FE model. These two models are mathematically different and thus special attention has to be paid to the coupling. In this study, different atomistic-to-continuum coupling options are numerically tested on a 1D coupled model. The performance of the following options was investigated: the strict and interpolated LMs, the local and non-local atomistic interaction, the weighting strategy and the weighting function.

The strict coupling, the more expensive option, gives exact results for the local atomistic interaction and shows neither dependence of the choice on the weighting function nor the size of the elements in the bridging zone. The strict coupling for the non-local interaction considerably

varies with the choice of the weighting function in the case of the weighting strategy A. On the other hand, for the weighting strategy B, the exact constant strain field is obtained for all weighting functions.

The interpolated coupling reduces the number of degrees of freedom by adding the interpolated LM field. This coupling yields errors for both local and non-local atomistic interaction. It significantly depends on the number of FEs in the bridging zone. It is thus recommended to use strict coupling at least in 1D and 2D cases due to accuracy. However, for 3D problems with many DOFs, the interpolated coupling should be considered to optimize the accuracy and the computational time.

It should be noted that for both the strict and the interpolated coupling the discrepancy from the constant strain field caused by GFs is a localized effect which does not influence the atomistic or continuum domain. Hence, it is possible to use the nSM technique as an approach to study nano-defects, but bearing in mind that the area of interest has to be far enough from the coupling domain.

In the future study, the weak form of displacement compatibility (often called L^2 and H^1) will be considered. This approach averages the coupling error, due to the integral form of the coupling constraint, but requires an additional approximation of the atomistic displacement. Furthermore, the force based coupling should be considered as in [29]. The displacement coupling presented herein and the force coupling represent upper (Voigt) and lower (Reuss) stiffness bounds, respectively [30]. The influence of the displacement and the force coupling on the stiffness will be studied in future. The research plan also includes two-dimensional (2D) and three-dimensional (3D) generalization of the proposed algorithm in order to be able to include the crack-like defects in the nano-submodel. In order to describe the material more realistic, the complex potentials, like the Brenner and Dreiding potential for carbon structures should be used. Furthermore, the use of the nSM technique is planned to be studied on nano-defects in carbon structures *e.g.* carbon nanosheets (2D), and carbon nanotubes (3D).

Acknowledgments

This study was supported by the Ministry of Science, Education and Sports of the Republic of Croatia within the framework of the research projects No 120-1201910-1812 and 120-1201910-1906.

REFERENCE

[1] Marenic, E., Skozrit, I., Tonkovic, Z., On the calculation of stress intensity factors and J-integrals using the submodeling technique, Journal of Pressure Vessel Technology 132 (4) (2010), p. 041203.

[2] Fish, J., Multiscale Methods Bridging the Scales in Science and Engineering, Oxford Univeristy press, 2009.

[3] Dhia, H. B., Rateau, G., The Arlequin method as a flexible engineering design tool, International Journal for Numerical Methods in Engineering 62 (2005), pp. 1442–1462.

[4] Dhia, H. B., Elkhodja, N., Roux, F.-X., Multimodeling of multi-alterated structures in the Arlequin framework. solution with a domain-decomposition solver, European Journal of Computational Mechanics 17 (2008), pp. 969 – 980.

[5] Qiao, H., Yang, Q., Chen, W., Zhang, C., Implementation of the Arlequin method into ABAQUS: Basic formulations and applications, Advances in Engineering Software 42 (4) (2011), pp. 197 – 207, ISSN 0965-9978.

[6] Ibrahimbegovic, A., Nonlinear Solid Mechanics, Springer, 2009.

[7] Sanchez-Palencia, E., Non-homogeneous media and vibration theory, Springer, 1980.

[8] Ibrahimbegovic, A., Markovic, D., Strong coupling methods in multi-phase and multi-scale modeling of inelastic behavior of heterogeneous structures, Computer Methods in Applied Mechanics and Engineering 192 (28-30) (2003), pp. 3089 – 3107, ISSN 0045-7825.

[9] Mullins, M., Dokainish, M., Simulation of the (001) plane crack in alpha-iron employing a new boundary scheme, Philosophical Magazine A 46 (1982), pp. 771–787.

[10] Kohlhoff, S., Gumbsch, P., Fischmeister, H. F., Crack propagation in b.c.c. crystals studied with a combined finite-element and atomistic model, Philosophical Magazine A 64:4 (1991), p. 851 878.

[11] Curtin, W. A., Miller, R. E., Atomistic/continuum coupling in computational materials science, Modelling Simul. Mater. Sci. Eng. 11 (2003), pp. 33–68.

[12] Harold S. Park, W. K. L., An introduction and tutorial on multiple-scale analysis in solids, Computer Methods in Applied Mechanics and Engineering 193 (2004), pp. 1733–1772.

[13] Liu, W. K., Karpov, E. G., Zhang, S., Park, H. S., An introduction to computational nanomechanics and materials, Computer Methods in Applied Mechanics and Engineering 193 (17-20) (2004), pp. 1529 – 1578, ISSN 0045-7825.

[14] Miller, R. E., Tadmor, E. B., A unified framework and performance benchmark of fourteen multiscale atomistic/continuum coupling methods, Modeling and Simulation in Materials Science and Engineering 17 (2009), p. 053001.

[15] Belytschko, T., Xiao, S. P., Coupling methods for continuum model with molecular model, International Journal for Multiscale Computational Engineering 1 (2003), p. 12.

[16] Xiao, S. P., Belytschko, T., A bridging domain method for coupling continua with molecular dynamics, Computer Methods in Applied Mechanics and Engineering 193 (17-20) (2004), pp. 1645 – 1669, ISSN 0045-7825.

[17] Guidault, P., Belytschko, T., Bridging domain methods for coupled atomistic-continuum models with l^2 or h^1 couplings, International Journal for Numerical Methods in Engineering 77-11 (2009), pp. 1566–1592.

[18] Bauman, P. T., Dhia, H. B., Elkhodja, N., Oden, J. T., Prudhomme, S., On the application of the arlequin method to the coupling of particle and continuum models, Computational Mechanics 42 (2008), pp. 511–530.

[19] Prudhomme, S., Dhia, H. B., Bauman, P., Elkhodja, N., Oden, J., Computational analysis of modeling error for the coupling of particle and continuum models by the Arlequin method, Computer Methods in Applied Mechanics and Engineering 197 (41-42) (2008), pp. 3399 – 3409, ISSN 0045-7825, recent Advances in Computational Study of Nanostructures.

[20] Allen, M. P., Tildesley, D. J., Computer simulation of liquids, Oxford Univeristy press, 1987.

[21] Griebel, M., Knapek, S., Zumbusch, G., Numerical Simulation in Molecular Dynamics, Springer, Berlin, Heidelberg, ISBN 978-3-540-68094-9, 2007.

[22] Elizondo, A. S., Horizontal Coupling in Continuum Atomistics, Ph.D. thesis, Fachbereich Maschinenbau und Verfahrenstechnik der Technischen Universitat Kaiserslautern, 2007.

[23] Ercolessi, F., A molecular dynamics primer, June 1997.

[24] Buehler, M. J., Atomistic Modeling of Materials Failure, Springer US, 2008.

[25] Belytschko, T., Gracie, R., Xu, M., A continuum-to-atomistic bridging domain method for composite lattices, International Journal for Numerical Methods in Engineering 81 (2010), pp. 1635–1658.

[26] Zhang, S., Mielke, S. L., Khare, R., Troya, D., Ruoff, R. S., Schatz, G. C., Belytschko, T., Mechanics of defects in carbon nanotubes: Atomistic and multiscale simulations, Phys. Rev. B 71 (11) (2005), p. 115403.

[27] Zhang, S., Khare, R., Lu, Q., Belytschko, T., A bridging domain and strain computation method for coupled atomistic-continuum modelling of solids, International Journal for Multiscale Computational Engineering 70 (2007), pp. 913–933.

[28] Miller, R. E., Tadmor, E. B., The quasicontinuum method: Overview, applications and current directions, Journal of Computer-Aided Materials Design 9 (2002), p. 203239.

[29] Fish, J., Nuggehally, M. A., Shephard, M. S., Picu, C. R., Badia, S., Parks, M. L., Gunzburger, M., Concurrent AtC coupling based on a blend of the continuum stress and the atomistic force, Computer Methods in Applied Mechanics and Engineering 196 (45-48) (2007), pp. 4548 – 4560.

[30] Markovic, D., Ibrahimbegovic, A., On micro-macro interface conditions for micro scale based FEM for inelastic behavior of heterogeneous materials, Computer Methods in Applied Mechanics and Engineering 193 (48-51) (2004), pp. 5503 – 5523.

Submitted: 10.10.2011

Accepted: 23.3.2012

Eduard Marenić
eduard.marenic@fsb.hr
Jurica Sorić
jurica.soric@fsb.hr
Zdenko Tonković
zdenko.tonkovic@fsb.hr
Faculty of Mechanical Engineering
and Naval Architecture,
University of Zagreb,
Ivana Lučića 5,
10 000 Zagreb, Croatia